Journal of Solid State Chemistry **161,** 135–151 (2001)
doi:10.1006/jssc.2001.9301, available online at http://www.idealibrary.com on IDEAL®

Quaternary Lead–Niobium–Tungsten Oxides Based on the Tetragonal Tungsten Bronze Structure

Sarah K. Haydon and David A. Jefferson[1]

Centre for Atomic Imaging, Department of Chemistry, University of Cambridge, Lensfield Road, Cambridge, CB2 1EW, United Kingdom

Received April 3, 2001; in revised form June 19, 2001; accepted July 12, 2001

High-resolution electron microscopy and diffraction studies of fully oxidized and reduced Pb–Nb–W–O oxides are presented. The phases observed were superstructures of tetragonal tungsten bronze (TTB), formed by ordering of pentagonal columns (PCs) and pentagonal tunnels (PTs). In fully oxidized preparations, the structure progressed from a quaternary $Nb_8W_9O_{47}$ analogue to the $K_5Nb_9W_2O_{31}$ structure, with an orthorhombic $\sim\sqrt{2}a_{TTB} \times \sqrt{2}a_{TTB} \times c_{TTB}$ TTB superstructure having two PCs per cell. Electron diffraction determined the true structure as a $2a_{TTB} \times 2a_{TTB} \times 2c_{TTB}$ supercell. With further lead incorporation, lead-filled PTs replaced PCs, forming a quaternary TTB analogue. Reduced quaternary phases were prepared by reacting lead with $Nb_8W_9O_{47}$. The structure was initially maintained in the quaternary phase, but converted at high-temperature to the $K_5Nb_9W_2O_{31}$ type. Excess lead caused the formation of lead-rich interfaces between domains. Reaction of lead with oxides in the ratio $4Nb_2O_5$:$9WO_3$ formed quaternary phases possessing the $Nb_8W_9O_{47}$ structure, demonstrating the direct synthesis of mixed PT/PC quaternary "bronze" phases which retained the structure of the oxidized ternary parent. © 2001 Academic Press

Key Words: **HREM; electron diffraction; EDS; octahedral tilt; supercell; $K_5Nb_9W_2O_{31}$; pentagonal column; pentagonal tunnel; quaternary tungsten–niobium oxides.**

1. INTRODUCTION

Ternary tungsten oxide systems can be grouped into two categories, namely reduced, non-stoichiometric tungsten bronzes and fully oxidized insulating phases (1, 2). Bronzes form when WO_3 is reduced, normally by exposure to the vapor of a guest or "impurity" metal. This reaction induces the oxide framework to distort or rearrange to incorporate the guest atoms. There are several possible resulting bronze structures possessing either square (3), pentagonal (4), or hexagonal (5, 6) tunnels, whose configurations are consequently stabilized by the accommodation of the guest metal within the framework. Fully oxidized analogues to bronzes form via the chemical substitution of some of the tungsten atoms with fully oxidized cations of a lower valence, e.g., the substitution of Nb^{5+} for W^{6+} in the Nb_2O_5–WO_3 system (7, 8). Bronzes characteristically exhibit deep, lustrous metallic-like colors (9) whereas the fully oxidized compounds are generally colorless (2).

For certain guest metal species (2) or degrees of Nb^{5+} substitution (8) the structures of ternary tungsten oxides are dominated by pentagonal tunnel (PT) (4), or if these are filled by infinite strings of metal and oxygen atoms, by pentagonal column (PC) (10, 11) formation. One of the distinctive features of PT/PC structures is that geometric factors require that the presence of one tunnel implies the formation of additional PTs or PCs (12, 13). Many fully oxidized ternary structures commonly contain a combination of both types of units, but the sole ternary bronze containing pentagonal units is tetragonal tungsten bronze (TTB) (4), shown in Fig. 1a, where PTs are partially filled by the guest metal atoms.

For PC phases, changes in stoichiometry are compensated via the generation of PCs within some pentagonal tunnels. This is typified by the Nb_2O_5–WO_3 system, where over a wide range of composition structures consist of vacant PTs and PCs coexisting within a TTB host framework. The variation in composition of these phases is achieved through changes in the ratio of PCs to empty PTs. Since PTs and PCs can be arranged in many ways, preparations of this type are typically disordered (14–16). However, at certain compositions ordered structures exist, such as $Nb_8W_9O_{47}$ (17), $Nb_4W_7O_{31}$ (18, 19), and Nb_2WO_8 (20). Of these only $Nb_8W_9O_{47}$ (henceforth referred to as 3-TTB) is based entirely on a TTB framework, possessing a simple three-fold superstructure where 4 out of 12 empty PTs are filled to produce PCs, as shown in Fig. 1b.

Guest metal atoms may be introduced into the empty PTs of a fully oxidized PC structure, thereby synthesizing a mixed PT/PC quaternary tungsten oxide. This can be achieved by the formal substitution of Nb^{5+} plus a monovalent cation for W^{6+} in the fully oxidized structure. The monovalent ion resides within vacant PTs and maintains

[1] To whom correspondence should be addressed. E-mail: daj4@cus.cam.ac.uk. Fax: +44 1223 336362.

0022-4596/01 $35.00

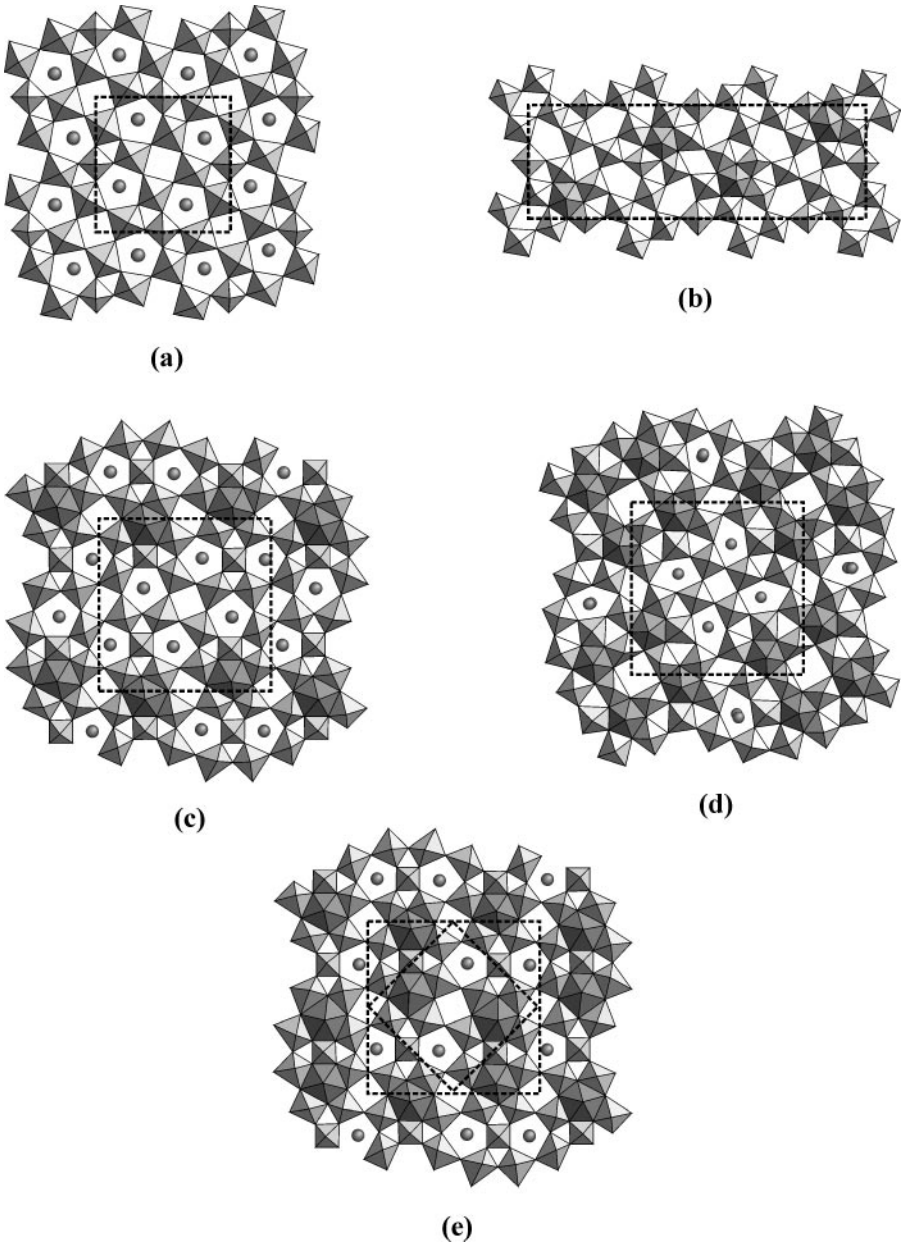

FIG. 1. [001] projections of (a) the basic TTB structure, $a = b \approx 12$ Å, $c \approx 3.8$ Å; (b) 3-TTB, $a \approx 36$ Å, $b \approx 12$ Å, $c \approx 3.8$ Å; (c) o-$\sqrt{2}$TTB; (d) t-$\sqrt{2}$TTB; (e) m-TTB. In all cases the repeat unit is indicated by dashed lines.

the electroneutrality of the structure. This principle has been explored for the Cs (21), K (22, 23), and Na (24–26) quaternary –Nb–W–O systems. These studies have identified several new PT/PC structures, including three TTB-related phases.

When $Cs_{0.7}Nb_{2.7}W_{2.3}O_{14}$ was synthesized, the structure was found to contain PCs, hexagonal, and seven-sided tunnels (21). High-resolution electron microscopy (HREM) studies of the $K_xNb_{8+x}W_{9-x}O_{47}$ series reported 3-TTB and a phase containing PCs and hexagonal tunnels (22). In addition, a TTB-related PT/PC phase $K_5Nb_9W_2O_{31}$ was identified which possesses a nearly tetragonal supercell based on TTB, with $a \approx b \approx \sqrt{2}a_{TTB}$ and $c \approx c_{TTB}$ (23). However, the true symmetry of the structure is orthorhombic, and it is referred to subsequently as o-$\sqrt{2}$TTB. This structure, which is isostructural with that of $K_5Nb_{11}O_{29}F_2$ (27), is shown in Fig. 1c.

In sodium-containing phases a disordered 3-TTB-type quaternary phase was most commonly observed. However, $NaNb_5WO_{16}$ was also characterized, possessing a tetragonal $a = b = \sqrt{2}a_{TTB}$ structure based on a PT/PC ordering scheme where one-half of all PTs are converted into PCs.

This structure, shown in Fig. 1d, will henceforth be referred to as t-$\sqrt{2}$TTB. $NaNb_5WO_{16}$ is isostructural with $KNb_{12}O_{29}F_3$ (28), and has the same framework structure as the ternary oxide $(Nb, W)_{12}O_{32}$ (29). In addition, a different PT/PC ordering scheme isostructural with $KNb_6O_{15}F$ (28) and H-KNb_3O_8 (30) was also observed. The structure of this phase, henceforth referred to as m-TTB, can be viewed ideally as an orthorhombic unit cell with $a \approx b \approx \sqrt{2}a_{TTB}$ although the structure is distorted and the true cell is monoclinic, with $a = c \approx 12.5$ Å and $\beta = 90.55°$. The arrangement of PCs and PTs in this structure is shown in Fig. 1e.

Another possible means of introducing guest metal atoms into the empty PTs of a fully oxidized PC structure is by the reduction, *in situ*, of a PC "precursor" framework, in a manner similar to bronze formation. Such compounds would represent "intermediate" PT/PC-type phases, lying between pure PT (bronzes) and pure PC structures (e.g., niobium–tungsten oxides). The formation of reduced phases by such a mechanism has not yet been extensively investigated, but in one such study, lithium was chemically and electrochemically inserted into the empty PTs of a 3-TTB precursor structure (31), and bronze-like compounds of the type $Li_xNb_8W_9O_{47}$ were formed.

This paper presents an investigation of fully oxidized and partially reduced Pb–Nb–W–O quaternary tungsten oxides. Although Pb–Nb–W–O phases have not been examined previously, there has been extensive characterization of the appropriate ternary compounds, namely lead tetragonal tungsten bronze, Pb_xWO_3 (lead-TTB) (32–34), ferroelectric $PbNb_2O_6$ (35–37), and PC-type niobium–tungsten oxides (17–20). Lead-TTB and $PbNb_2O_6$ both possess the PT TTB structure (Fig. 1a) and indicate the preference of lead for creating and filling PTs.

The fully oxidized samples synthesized are based on the compositional analogue ($Pb_{0.35}Nb_{2.7}W_{2.3}O_{14}$) of the novel PT/PC phase $Cs_{0.7}Nb_{2.7}W_{2.3}O_{14}$ (21). A series of samples were prepared by incrementally increasing the number of guest metal cations available in the reaction, while the Nb–W–O framework composition was kept constant. Samples of general formula $Pb_xNb_{1.17}W_{1.0}O_{5.93+x}$ ($0 \leq x \leq 0.87$) were prepared.

Reduced quaternary phases were prepared via two strategies. In a series of "precursor" preparations, the structural consequences of heating lead in the presence of a preexisting tungsten–niobium PC framework were investigated. 3-TTB was chosen as the precursor since it possesses vacant PTs suitable for accommodating lead. In "component" preparations 3-TTB was synthesized directly from Nb_2O_5 and WO_3 in the presence of small quantities of lead.

2. EXPERIMENTAL

Fully oxidized phases were synthesized from appropriate quantities of $PbWO_4$, WO_3 (Johnson Matthey, 99.8%), and Nb_2O_5 (Aldrich, 99.9%). $PbWO_4$ was prepared from pellets of PbO (Aldrich, also 99 + %) and WO_3 heated at 800°C for 3 days. Finely ground mixtures were sealed inside unevacuated silica ampoules and heated at 950°C for periods of 5 days. The ampoules were contained inside steel bombs during heating in case of tube failure, and their nonevacuation ensured that samples were not subjected to a reducing atmosphere. After heating, all samples were white or pale yellow powders, indicating that the cations were in their highest oxidation state.

The 3-TTB precursor was prepared by heating a mixture of Nb_2O_5 and WO_3 in a sealed unevacuated silica tube at 1000°C for 5 days. Reduced precursor phases were synthesized by heating quantities of the 3-TTB so produced ($Nb_{0.89}WO_{5.2}$) with various quantities of Pb (AnalaR, 99.97%) in sealed evacuated silica tubes to ensure nonoxidation of the metal. Specimens of the series $Pb_xNb_{0.89}WO_{5.2}$ with $x = 0.03$, 0.34, 0.68, 1.35, were prepared at 750°C for 7 days. Two further specimens for $x = 0.34$ and 0.68 were heated at 1000°C for 7 days. After synthesis, the pale yellow of the precursor was replaced by a dark blue "chalky" appearance in the $x = 0.03$ specimen, and a deep, blue/black lustrous appearance for all other compounds. Residual lead was observed in some samples after heating.

Component preparations were synthesized by heating lead in sealed evacuated silica tubes with Nb_2O_5 and WO_3 in a 4:9 ratio. Samples of the series $Pb_xNb_{0.89}WO_{5.2}$ for $x = 0.03$ and 0.09 were synthesized by heating at 1000°C for 2 days. A further sample ($x = 0.09$) was heated at 1000°C for 7 days so that the effect of more prolonged synthesis could be investigated.

Characterization was performed using powder X-ray diffraction (PXRD), HREM, selected area electron diffraction (SAED), and energy dispersive X-ray spectroscopy (EDS). PXRD studies employed a Stoe horizontal diffractometer working in transmission mode (Cu$K\alpha$, $\lambda = 1.5456$ Å). For the diffractometer small quantities of each sample were mounted on transparent adhesive tape which was inserted in a disc-like holder. Images and diffraction patterns were recorded using a JEM-200CX electron microscope with an ultra-high-resolution specimen stage and objective lens ($C_S = 0.36$, $C_C = 0.65$) (38, 39) and a standard JEM-2010 instrument ($C_S = 0.50$, $C_C = 1.10$), both operated at 200 kV. Image simulations were performed using customised software (40). Specimens for microscopy were first embrittled under liquid N_2 and subsequently ground in acetone suspension. A drop of this was dispersed on a holey carbon film supported on a standard specimen grid. Quantitative EDS measurements were recorded using a PGT beryllium window detector, calibrated with previously prepared standards of $PbWO_4$ and $Nb_8W_9O_{47}$ (3-TTB) to determine the relative detector efficiency for the W$L\alpha$, Pb$L\alpha$, and Nb$K\alpha$ lines.

TABLE 1
Combined EDS and HREM Results for Fully Oxidized Phases

Sample	Nominal composition $Pb_xNb_{1.17}W_{1.0}O_{5.93+x}$	Averaged experimental composition	Structure	Minority phases[a]
1	$Nb_{1.17}W_{1.0}$	$Nb_{2.11\pm0.18}W_{1.0}$	Nb_2WO_8	—
		$Nb_{1.14\pm0.10}W_{1.0}$	3-TTB (domains)	
2	$Pb_{0.15}Nb_{1.17}W_{1.0}$	$Pb_{0.12\pm0.01}Nb_{1.19\pm0.08}W_{1.0}$	3-TTB + o-$\sqrt{2}$TTB	—
3	$Pb_{0.30}Nb_{1.17}W_{1.0}$	$Pb_{0.26\pm0.04}Nb_{1.22\pm0.13}W_{1.0}$	o-$\sqrt{2}$TTB	—
4	$Pb_{0.44}Nb_{1.17}W_{1.0}$	$Pb_{0.31\pm0.05}Nb_{1.37\pm0.17}W_{1.0}$	o-$\sqrt{2}$TTB	$Pb_{0.47}Nb_{1.02}W_{1.0}$
5	$Pb_{0.59}Nb_{1.17}W_{1.0}$	$Pb_{0.41\pm0.05}Nb_{1.65\pm0.15}W_{1.0}$	o-$\sqrt{2}$TTB	$Pb_{0.72}Nb_{0.85}W_{1.0}$
6	$Pb_{0.74}Nb_{1.17}W_{1.0}$	$Pb_{0.67\pm0.11}Nb_{1.50\pm0.17}W_{1.0}$	o-$\sqrt{2}$TTB	$Pb_{0.77\pm0.07}Nb_{0.76\pm0.15}W_{1.0}$
				$Pb_{0.53}Nb_{0.33}W_{1.0}$
7	$Pb_{0.87}Nb_{1.17}W_{1.0}$	$Pb_{0.82\pm0.07}Nb_{1.58\pm0.15}W_{1.0}$	o-$\sqrt{2}$TTB	$Pb_{0.84}Nb_{1.05}W_{1.0}$
				$Pb_{0.17}Nb_{0.75}W_{1.0}$

[a] Averaged composition of minority phases, most with insufficient data to determine an error in the measurement.

The homogeneity of the prepared standard materials was initially checked by PXRD, but in order to obtain reasonable statistics and to check the homogeneity of these materials further, 50 point analyses were obtained for $PbWO_4$ and 85 for $Nb_8W_9O_{47}$. The effects of absorption errors were monitored by noting the value of the intensity ratio for the WM and W$L\alpha$ lines in both standards, and where this value was abnormally low the measurement was not included in the final determination. Similarly, any analyses with W$L\alpha$/Nb$K\alpha$ or W$L\alpha$/Pb$L\alpha$ intensity ratios differing markedly from the norm were also rejected. Final standard deviations in the intensity ratios for the two standards were $\pm$ 4.0% and $\pm$ 3.9%, respectively. Between 35 and 40 analyses were obtained for each unknown specimen studied, and the same absorption criterion was applied. In this case however, where the specimen homogeneity was by no means certain, an attempt was made to group analyses together as being representative of the different phases which might be present.

3. RESULTS AND DISCUSSION

3.1. Fully Oxidized Phases

PXRD patterns from these samples could be indexed mainly on the basis of the $x = 0$ phase ($Nb_8W_9O_{47}$) and the $PbWO_4$ reagent, although there were several reflections which could not be assigned to either phase. EDS studies, however, indicated a quaternary Pb–Nb–W–O majority phase with a composition varying with x (Table 1), some $PbWO_4$, and occasionally WO_3. For $x = 0$, two Nb:W ratios were observed, one being very similar to the composition expected from the starting material and a second (Nb:W $\approx$ 2:1) which suggested the formation of Nb_2WO_8, a PC phase not related to TTB (20). The results for samples with $x > 0$ revealed an overall trend of increasing Pb and Nb content, but whereas the Pb content increased for all compositions, the amount of Nb present reached a maximum at $x = 0.59$. All samples with $x \geq 0.44$ contained small quantities of other quaternary phases.

Electron diffraction from the sample with $x = 0$ confirmed the presence of small quantities of Nb_2WO_8. The majority phase observed, however, was the disordered 3-TTB structure. Here, the three-fold TTB superstructure reflections were affected by "circular diffuse scattering," shown in Fig. 2, which is indicative of disorder among the PC distribution within the TTB framework (14–16). Equivalent SAED patterns from the $x = 0.15$ sample also exhibited pools of diffuse scattering around the TTB subcell reflections (Fig. 3), and three structural domains (labelled A to C) could be identified in the image of this crystal, as indicated in Fig. 3. Power spectra (PS) calculated from each region are shown in Figs. 3A–3C. The image of region A is disordered and correspondingly its PS comprises TTB subcell maxima surrounded by diffuse scattering. The PS of region B displays two peaks between those from the TTB subcell, identifying this domain as a 3-TTB intergrowth, whereas the PS

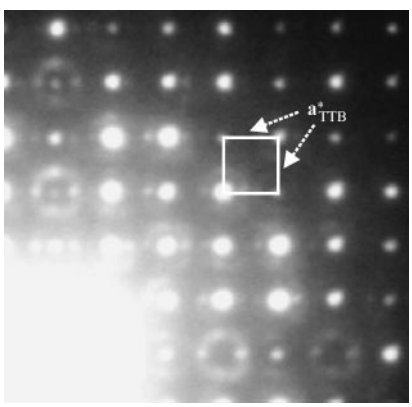

FIG. 2. [001] SAED pattern enlargement from the $x = 0$ sample. The radius of circular diffuse scattering around each TTB subcell reflection equates to one-third the a^*_{TTB} repeat.

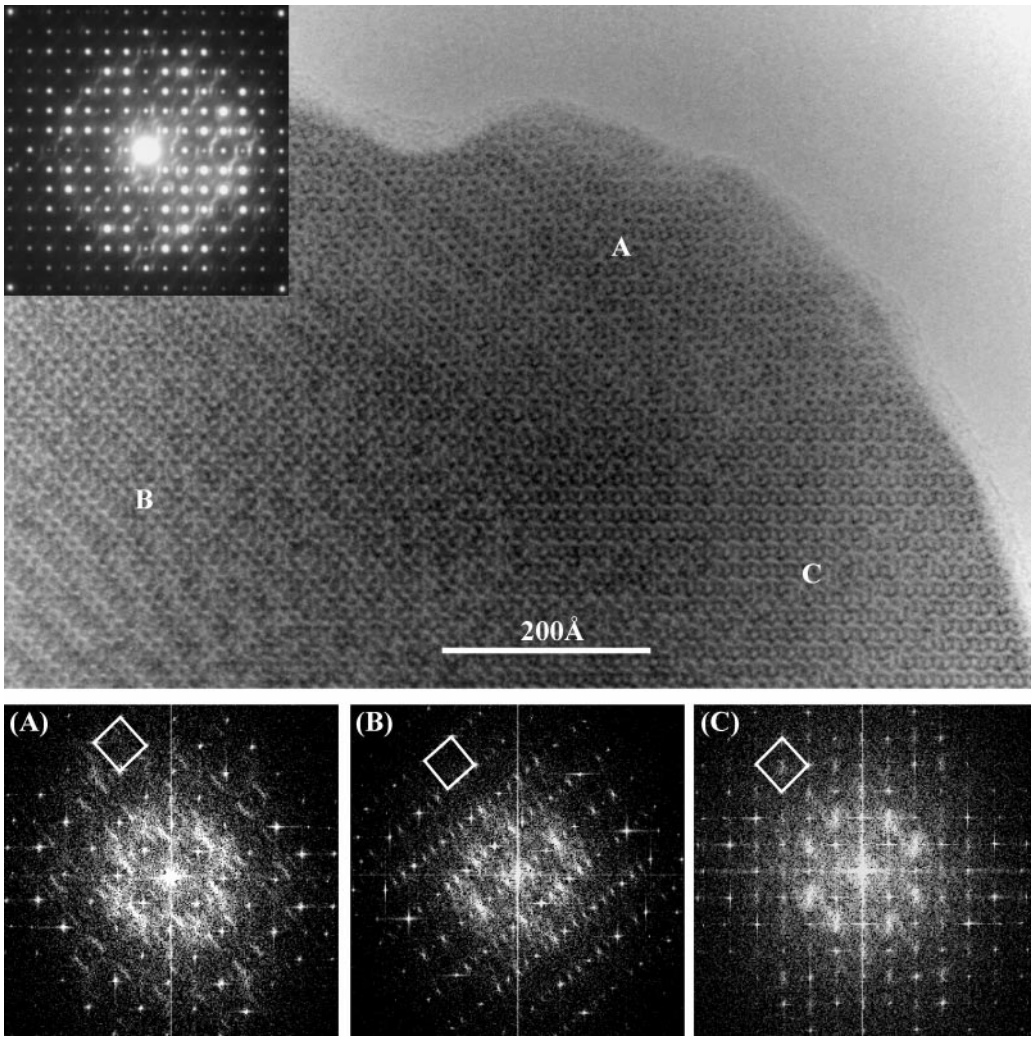

FIG. 3. Example HREM image and SAED pattern from sample $x = 0.15$ including power spectra of regions A, B, and C. White square indicates basic TTB subcell periodicity.

for region C also displays the TTB subcell, but has an additional diffuse peak at the center of the basic TTB square. The separation of fringes in region C was measured as $a \approx b \approx 17$ Å ($\approx\sqrt{2}a_{\mathrm{TTB}}$), which is in agreement with the EDS diffraction data (discussed below). This evidence suggested that domain C was an intergrowth of an approximate $\sqrt{2}a_{\mathrm{TTB}} \times \sqrt{2}a_{\mathrm{TTB}}$ TTB-type superstructure ($\sqrt{2}$-TTB).

Analysis of samples with $x > 0.15$ indicated that ordered crystals containing only the $\sqrt{2}$-TTB phase were formed with an increased lead content, as shown in Fig. 4a. Asymmetric SAED patterns recorded from these $\sqrt{2}$-TTB crystals also exhibited systematically weak odd-order Laue layers lying half-way between the positions of the strong even-order layers, the latter corresponding to the basic 3.8 Å c_{TTB} repeat (Fig. 4b). Patterns from a range of samples were analyzed using a method devised to interpret reciprocal lattice periodicities in adjacent Laue levels of asymmetric SAED patterns (41), this indicating that these weak odd-order reflections were present in the same positions as the maxima in the even layers, but also at the midpoint of each edge of the basic TTB square. These are shown in the inset in Fig. 4b, and imply a true cell periodicity of $a_{\mathrm{ss}} = 2a_{\mathrm{TTB}}$, $b_{\mathrm{ss}} = 2b_{\mathrm{TTB}}$, and $c_{\mathrm{ss}} = 2c_{\mathrm{TTB}}$, i.e., a "$2 \times 2 \times 2$" TTB superstructure.

Whenever possible, both asymmetric SAED patterns and EDS spectra were recorded from the crystals analyzed. Figure 5 shows such results from a crystal of quaternary composition from the sample with nominal composition Pb = 0.74 (Table 1). The composition of the crystal agrees well with the average of the majority of quaternary phase readings from this sample. Similar patterns were obtained from all preparations with $x > 0.15$ and always corresponded to crystals of a quaternary phase. Measurement of these patterns indicated an $a \approx b \approx 17$ Å repeat unit from the

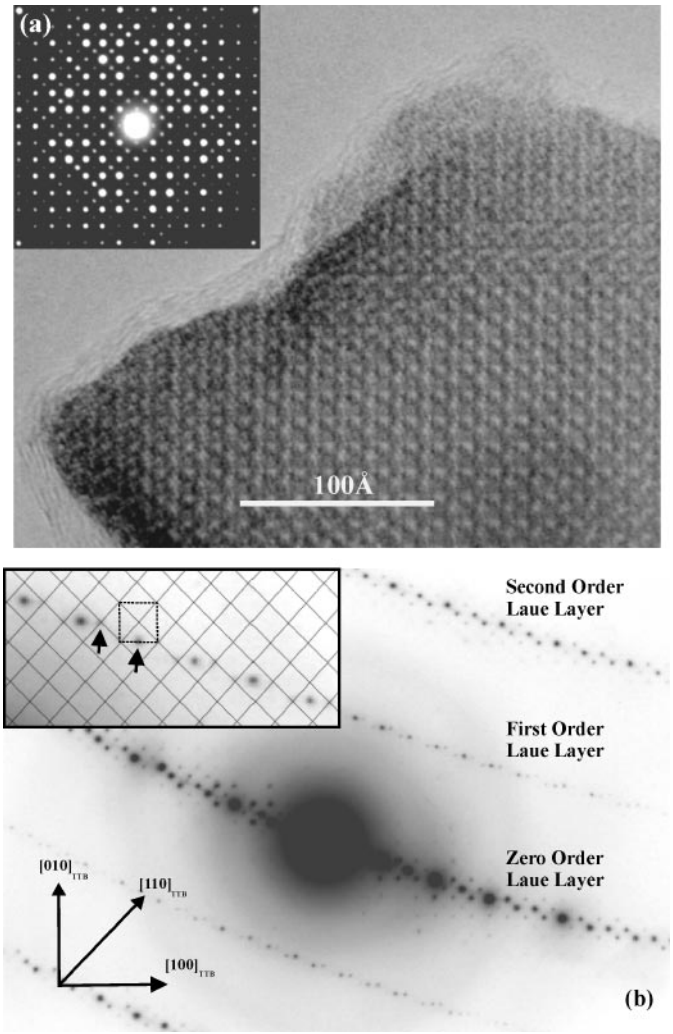

FIG. 4. (a) HREM image and SAED pattern of the $\sqrt{2}$-TTB phase (sample $x = 0.30$). (b) Asymmetric diffraction pattern of the $\sqrt{2}$-TTB phase. In the inset enlargement of the first-order Laue layer, the black mesh defines the $\sqrt{2}$-TTB reciprocal lattice periodicity (41), and the dashed square illustrates the position of the basic TTB cell repeat with respect to the $\sqrt{2}$-TTB cell.

zero-order Laue layers. Quaternary phase SAED patterns were very distinct from those of the ternary minority phases observed ($PbWO_4$, WO_3), and thus the observation of DPs similar to Fig. 5 could be unambiguously assigned to quaternary phases. Table 1 summarizes the compositional and structural findings for the complete series of samples.

Discussion. Both the o-$\sqrt{2}$TTB and t-$\sqrt{2}$TTB structures (Figs. 1c and 1d) possess [001] electron diffraction patterns similar to those observed for the Pb–Nb–W–O $\sqrt{2}$-TTB phase (23, 28). The m-TTB structure can be discounted as a possibility since its diffraction pattern appears with only basic TTB reflections (28) and since the deviation from an orthogonal lattice is small, its zero-order [001] SAED pattern appears almost identical to that of TTB.

Distinguishing between the o-$\sqrt{2}$TTB and t-$\sqrt{2}$TTB structures using only SAED patterns is difficult, since the orthorhombic distortion of o-$\sqrt{2}$TTB is very small, and the intensity distribution in [001] diffraction patterns from each phase is very similar (23). However, consideration of the theoretical and experimental compositions enables the structure type to be identified unambiguously.

Compositional considerations. The compositions of the o-$\sqrt{2}$TTB and t-$\sqrt{2}$TTB cells are $A_6M_{22}O_{62}$ and $A_4M_{24}O_{64}$ respectively, where A is the guest metal inhabiting PTs and M the combined number of Nb and W atoms of the framework and PCs. EDS indicates that the framework composition of the observed $\sqrt{2}$-TTB structure is such that all phases are Nb rich and have Nb:W ratios between 1 and 2 (Table 1). Furthermore, since all specimens are fully oxidised, it can be assumed that all cations are in their highest oxidation state (i.e., Nb^{5+}, W^{6+}, and Pb^{2+}). As Pb^{2+} is much larger than either Nb^{5+} or W^{6+} [1.18 Å compared with ca. 0.5 Å (42)] it is unrealistic to expect any oxygen to reside in PTs which are filled by Pb^{2+}.

For the t-$\sqrt{2}$TTB structure, where the unit cell contains four PCs and four PTs, there are 24 "framework" cations and 64 O^{2-} ions, and hence the maximum valence of the framework cations cannot exceed 5.33, even if there are no A species present. This would require a minimum Nb:W ratio of 2:1. However, experimentally determined ratios are always below this value, and furthermore, Pb^{2+} ions are also present, which implies that the framework charge would always *exceed* the magnitude of the negative charge from the anion framework (-128). Consequently the t-$\sqrt{2}$TTB phase therefore cannot form at the observed framework compositions.

If, on the other hand, the o-$\sqrt{2}$TTB phase is considered, the unit cell contains only two PCs and six PTs, giving a total of 22 framework cations and 62 anions. Under these circumstances the minimum average valence of the framework cations must be 5.64 if there are no A species present, and consequently for a Nb:W ratio between 1 and 2 the

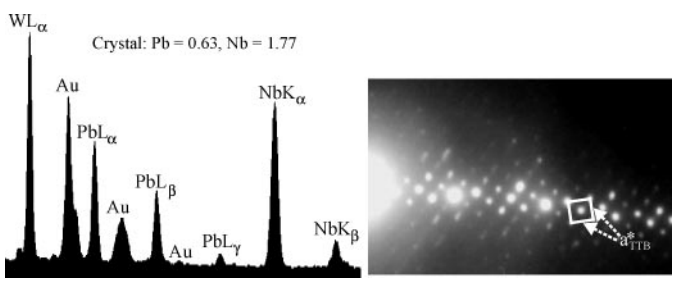

FIG. 5. EDS spectrum and off-tilt SAED pattern from sample $x = 0.74$ with true majority phase average composition Pb = 0.67 ± 0.11 and Nb = 1.50 ± 0.17 (gold specimen grid).

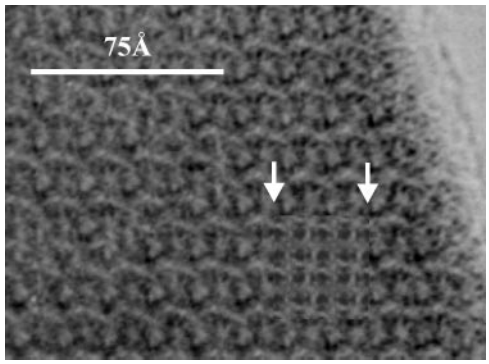

FIG. 6. Example image simulation of the o-$\sqrt{}$2TTB structure using region C from Fig. 3: 139 Å, $\Delta f = 50$ Å.

framework charge is always less than the magnitude of charge due to the anions. Hence, all the observed compositions require incorporation of Pb cations into PTs to preserve electroneutrality. The o-$\sqrt{}$2TTB structure is therefore the only $\sqrt{}$2-TTB model compatible with the observed compositional data. Matching of simulated images of the [001] projection of o-$\sqrt{}$2TTB with those obtained experimentally also supported these findings (Fig. 6), although when the PTs are filled differences between images of the o-$\sqrt{}$2TTB and t-$\sqrt{}$2TTB structures are minimal.

Interpretation of EDS results. The fully oxidized preparations were synthesized with a fixed Nb:W ratio and increasing Pb concentration. If the phases formed are part of a substitution series where $2Nb^{5+}$ and Pb^{2+} substitute for $2W^{6+}$, then an increase of the lead content should be accompanied by a corresponding increase in niobium and a decrease in tungsten contents. EDS data does initially demonstrate an increasing Pb:W and Nb:W ratio, but the observed maximum in the Nb:W ratio (whilst Pb:W continues to increase) suggests that a more complex process is occurring.

Table 1 shows that the o-$\sqrt{}$2TTB structure accommodates wide variations in both lead content and framework composition, and that it evolves from the 3-TTB structure as the quantity of lead incorporated increases. Sample 2 represents an intermediate step in this process as intergrowths of both structures were observed (Fig. 3). The replacement of 3-TTB by o-$\sqrt{}$2TTB can be rationalized by considering relative numbers of PCs and PTs within each cell. Since o-$\sqrt{}$2TTB contains more PTs (75%) compared to 3-TTB (66%), more Pb can be accommodated in the o-$\sqrt{}$2TTB structure.

The maximum theoretical composition of each structure can be written as $Pb_6^{PT}(MO)_2^{PC}M_{20}^{F}O_{60}^{F}$ for o-$\sqrt{}$2TTB and $Pb_8^{PT}(MO)_4^{PC}M_{30}^{F}O_{90}^{F}$ for 3-TTB where M = Nb, W and the superscripts PT (pentagonal tunnel), PC (pentagonal column), and F (framework) define the location of each component of the structure. Subsequent increases in lead incorporation beyond the limit defined by the number of PTs must begin to erode the PC distribution and necessitate the replacement of some PCs with lead-filled PTs. The limit for both structures occurs when all the PCs are replaced and a pure PT TTB-like phase is formed with composition $Pb_4^{PT}M_{10}^{F}O_{30}^{F}$.

The 3-TTB phase in sample 1 (Table 1) has a Nb:W ratio greater than that for ideal $Nb_8W_9O_{47}$ (Nb:W = 0.89) and therefore extra PCs must be present in the structure. Using the experimentally determined Nb:W ratio, the average cation valence (V_c) equates to 5.47. If the number of PCs is n, then there are $30 + n$ cations and $90 + n$ anions in total within the cell. Equating cation and anion valencies gives $n = 4.61$, and as there are normally four PCs within the cell, the implication is that there are 0.61 excess PTs, on average, in each cell that are converted into PCs. This result is supported by the observed disorder in images from this sample. The overall cell stoichiometry for this phase based on 34.61 cations per cell is then $Nb_{18.44}W_{16.17}O_{94.61}$, within the limits of accuracy of the EDS analysis, which is approximately 9%.

Sample 2 can be analyzed similarly, except that lead incorporation and the observation of both 3-TTB and o-$\sqrt{}$2TTB structures must be accounted for. For a determined Nb:W ratio of 1.19, the average M cation (i.e., niobium and tungsten atoms in M^F and M^{PC} sites) valence is 5.46, and 45.67% of $30 + n$ M cations will be tungsten. For a Pb:W ratio of 0.12, the number of lead atoms will be 12% of this, and if we assume all the lead to be present in the divalent state, equating cation and anion valencies gives a value for n of 3.65. The number of lead atoms per cell is then 1.84. Hence there are 3.65 PCs (which is less than the ideal number for 3-TTB) and 1.84 lead-filled PTs per cell. The overall cell composition for sample 2, again within the limits of error in the experimental ratios, is therefore $Pb_{1.84}Nb_{18.28}W_{15.37}O_{93.65}$.

For a lead-filled o-$\sqrt{}$2TTB structure in sample 2 the analysis is similar but there are $20 + n$ framework cations and $60 + n$ anions in the smaller unit cell, giving a value of $n = 2.43$ and the nubmer of lead atoms per cell as 1.23, implying 0.43 excess PCs and 1.23 lead-filled PTs per o-$\sqrt{}$2TTB. The overall o-$\sqrt{}$2TTB cell composition is then $Pb_{1.23}Nb_{12.19}W_{10.24}O_{62.43}$. This analysis agrees well with HREM evidence for intergrowths of both the 3-TTB and o-$\sqrt{}$2TTB structures in sample 2.

The results of the same calculation applied to the major phases of samples 1 to 7 are shown in Table 2. Samples 2 to 5 possess approximately the correct number of PCs per cell required for o-$\sqrt{}$2TTB (at around 2), and the lead content of these samples increases as more PTs become filled. The composition attained at sample 5, however, appears to represent the maximum lead incorporation tolerated by the o-$\sqrt{}$2TTB structure without replacing PC units by PTs, and

TABLE 2
Results of Cell Composition Calculations for Major Phases in Samples 1 to 7

Sample	Experimental cation ratios	Number of PCs	Number of lead-filled PTs	Cell composition
1 (3-TTB)	0:1.14:1.0	4.61	0	$Nb_{18.44}W_{16.17}O_{94.61}$
2 (3-TTB)	0.12:1.19:1.0	3.65	1.84	$Pb_{1.84}Nb_{18.28}W_{15.37}O_{93.65}$
(o-$\sqrt{2}$TTB)		2.43	1.23	$Pb_{1.23}Nb_{12.19}W_{10.24}O_{62.43}$
3 (o-$\sqrt{2}$TTB)	0.26:1.22:1.0	1.71	2.54	$Pb_{2.54}Nb_{11.93}W_{9.78}O_{61.72}$
4 (o-$\sqrt{2}$TTB)	0.31:1.37:1.0	1.72	2.84	$Pb_{2.84}Nb_{12.56}W_{9.16}O_{61.72}$
5 (o-$\sqrt{2}$TTB)	0.41:1.65:1.0	1.70	3.36	$Pb_{3.36}Nb_{13.51}W_{8.19}O_{61.70}$
6 (o-$\sqrt{2}$TTB)	0.67:1.5:1.0	0.33	5.45	$Pb_{5.45}Nb_{12.20}W_{8.13}O_{60.24}$
7 (o-$\sqrt{2}$TTB)	0.82:1.58:1.0	0	6.32	$Pb_{6.32}Nb_{12.18}W_{7.71}O_{59.88}$

corresponds to a maximum occupancy of each PT of approximately 50%. For samples 6 and 7 the number of PCs rapidly decreases to zero, implying that lead replaces all $(MO)^{PC}$ units, and consequently the niobium content stabilizes. At this point the structure therefore becomes more like a fully oxidized simple TTB analogue.

The excess W generated by the formation of a quaternary phase richer in niobium than the starting composition can combine with M^{PC} cations (Nb^{5+}, W^{6+}) liberated by lead substitution and form other frameworks that will be tungsten rich. This provides an explanation for the increasing occurrence of the tungsten-rich minority quaternary phases listed in Table 1.

Fully oxidized quaternary TTB. The majority of SAED patterns recorded from samples 6 and 7 possessed the extra $\sqrt{2}a^*_{TTB}$ reflection of o-$\sqrt{2}$TTB that was seen for the other compositions, and therefore the formation of a simple quaternary TTB phase (Q-TTB) was not initially suspected. However, the images recorded from these phases revealed a domain structure. In Fig. 7 two structure types can be identified (regions A and B). Power spectra analysis of this image demonstrates that region B possesses the additional maxima characteristic of the $\sqrt{2}$ structure whereas region A does not. The fringe periodicity ratio of region A to B equals 0.68, which is close to the expected value ($a_{TTB}/\sqrt{2}a_{TTB} = 0.7$), implying that region A corresponds to the Q-TTB phase and region B to the o-$\sqrt{2}$TTB structure. Region A cannot correspond to the pseudo-TTB PC phase m-TTB, since the high lead content precludes the formation of sufficient PCs.

The $2\times2\times2$ supercell of o-$\sqrt{2}$TTB. No doubled *c*-repeat and superstructure was reported for the $K_5Nb_9W_2O_{31}$ o-$\sqrt{2}$TTB phase (23), but studies of Na–Nb–W–O phases did report weak doubled *c* periodicities in some SAED patterns (25, 26), and odd-order Laue layer superstructures have been observed and characterized in studies of some TTB bronzes (34, 43–45) and TTB ferroelectric phases (e.g., 46, 47). Of particular relevance to Pb–Nb–W–O phases is the observation of large supercells on non-zero Laue layers in the related ternary phases of lead-TTB (34) and $PbNb_2O_6$ (35–37). The origin of these superstructures was linked with octahedral tilt and distortion within the framework, accompanied by partial occupancy and splitting of guest metal atom sites within the PTs. A single-crystal XRD structure of lead-TTB (34) revealed that the "true" average structure of a $Pb_{0.26}WO_3$ crystal

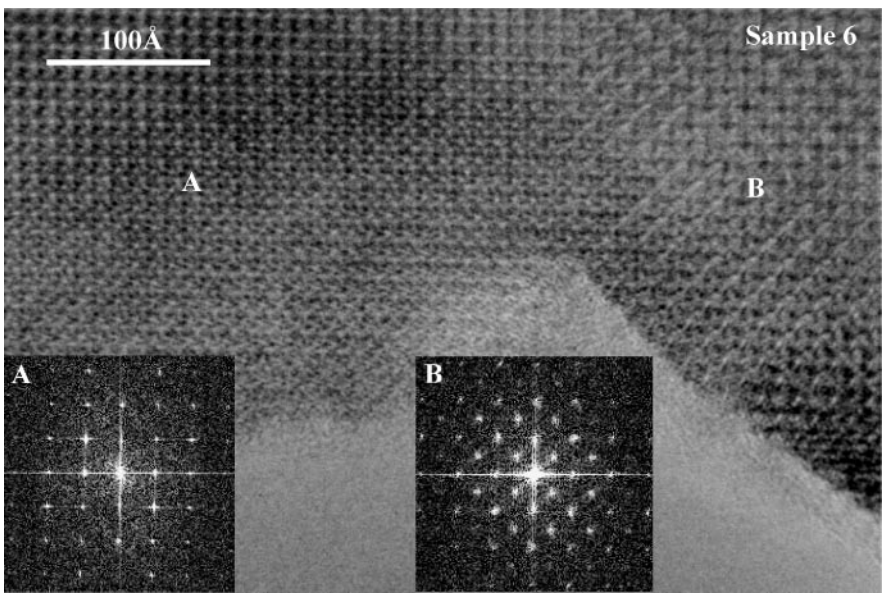

FIG. 7. HREM image and power spectrum of an intergrowth between Q-TTB (region A) and o-$\sqrt{2}$TTB (region B).

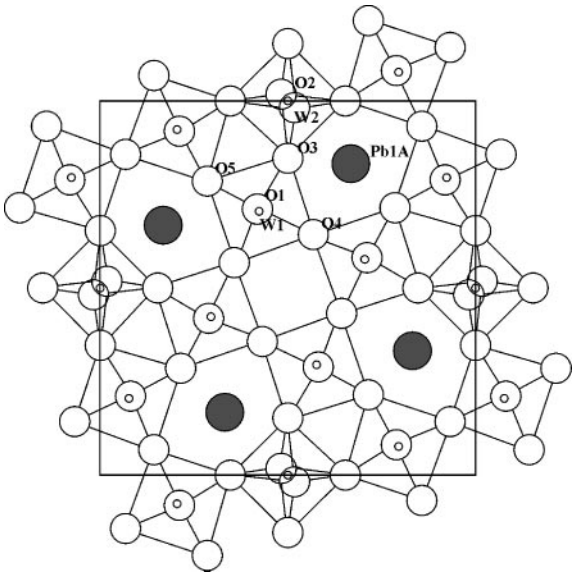

FIG. 8. The average lead-TTB structure [after Triantfyllou *et al.* (34)]. $a_{av} = b_{av} = 12.2$ Å, $c_{av} = 3.8$ Å and only the main lead positions are shown.

contained lead atoms split over three sites within each PT, coupled with a puckering of all equatorial oxygens with respect to the *ab* plane. As well as equatorial disorder, the apical oxygens of the octahedra lying in the center of the cell edges (O2) was found to be split along the [110] direction of the basic unit cell. This observation implied that the $M(2)O_6$ octahedron is tilted such that its axis is no longer parallel to *c* and a doubling of the unit cell along [001] is produced. A similar and more extensive pattern of tilted octahedra was also observed by Goreaud *et al.* (45) in their single-crystal XRD study of tin-TTB. The nature of this splitting of sites in the lead-TTB structure is shown in Fig. 8.

Since o-$\sqrt{2}$TTB possesses the same underlying TTB framework it would be expected that similar distortions of the octahedra would be present. However, the effect of the presence of PC units within the framework must also be taken into account. Consideration of the simple o-$\sqrt{2}$TTB structure (Fig. 9a) demonstrates that the severely tilted octahedron in the study of lead-TTB [$M(2)O_6$] lies in two different environments in this framework. One site is similar to that found in TTB, where $M(2)O_6$ is situated between two PTs but the second site places $M(2)O_6$ between a PC and a PT. This latter coordination environment is likely to constrain the tilt of $M(2)O_6$, because PC units must be in identical positions in both layers of a doubled cell so that the –M–O–M–O– linkage is preserved, and furthermore if the $M(2)O_6$ unit tilts then an associated tilting of the PC itself is implied, and this in turn must be restricted by the other surrounding octahedra. It is unlikely, therefore, that the $M(2)O_6$ octahedron can tilt in the same way that is found for lead-TTB, if at all. Thus, the presence of these PC units within the framework will limit possible tilting schemes. Consequently, if the complex superstructure of o-$\sqrt{2}$TTB is assumed to be caused only by the tilt of the first $M(2)O_6$ octahedron between PTs, it is readily possible to generate the required $2 \times 2 \times 2$ supercell, as shown in Fig. 9b.

Assuming statistical lead occupancies, the overall structure factor consists of contributions from the cation and oxygen atom frameworks: $F(hkl) = F_M(hkl) + F_O(hkl)$. If the distribution of niobium and tungsten is also assumed to be statistical, then the $2 \times 2 \times 2$ supercell contains four equivalent $(MO)_2M_{20}$ units of the o-$\sqrt{2}$TTB structure at (0, 0, 0), ($\frac{1}{2}$, $\frac{1}{2}$, 0), (0, 0, $\frac{1}{2}$), and ($\frac{1}{2}$, $\frac{1}{2}$, $\frac{1}{2}$). Therefore, the contribution to the overall structure factor from the framework cations is

$$F_M(hkl) = \sum_1^{N_M/4} f_M \exp 2\pi i(hx_M + ky_M + lz_M)[1 + \exp \pi i(l)] \times [1 + \exp \pi i(h + k)],$$

where N_M is the number of Nb and W atoms. Consequently, beams are absent unless l and $h + k$ are even, and cation scattering makes no contribution to odd-order Laue layers. On even-order layers maxima are predicted at positions corresponding to the corners and center of the basic TTB cell (Fig. 9c). This agrees with the observed zero-order layer diffraction patterns.

Identical arrays of the anion framework are, however, located at the positions (0, 0, 0) (0, $\frac{1}{2}$, 0), ($\frac{1}{2}$, 0, $\frac{1}{2}$), and ($\frac{1}{2}$, $\frac{1}{2}$, $\frac{1}{2}$). Hence the contribution from the anion framework is

$$F_O(hkl) = \sum_1^{N_O/4} f_O \exp 2\pi i(hx_O + ky_O + lz_O)\,[1 + \exp \pi i(k)] \times [1 + \exp \pi i(h + l)],$$

where N_O is the number of oxygen atoms. Oxygen scattering thus contributes to both odd and even Laue layers. When l is even, both h and k must be even for maxima to occur and hence only the basic TTB reflections occur. For l odd, however, k must be even and h odd, and maxima lying half-way along one side of the TTB square in the even layer (Fig. 9d) will be observed.

The reciprocal lattice for this model generates only half the number of observed supercell reflections on odd Laue levels. In experimental patterns weak odd-order reflections corresponding to the original o-$\sqrt{2}$TTB cell were observed together with main supercell reflections positioned half-way along *all* sides of the TTB square (Fig. 4b). The missing supercell reflections can be produced by a *second* similar supercell (Fig. 10a), where

$$F_O(hkl) = \sum_1^{N_O/4} f_O \exp 2\pi i(hx_O + ky_O + lz_O)\,[1 + \exp \pi i(h)] \times [1 + \exp \pi i(k + l)].$$

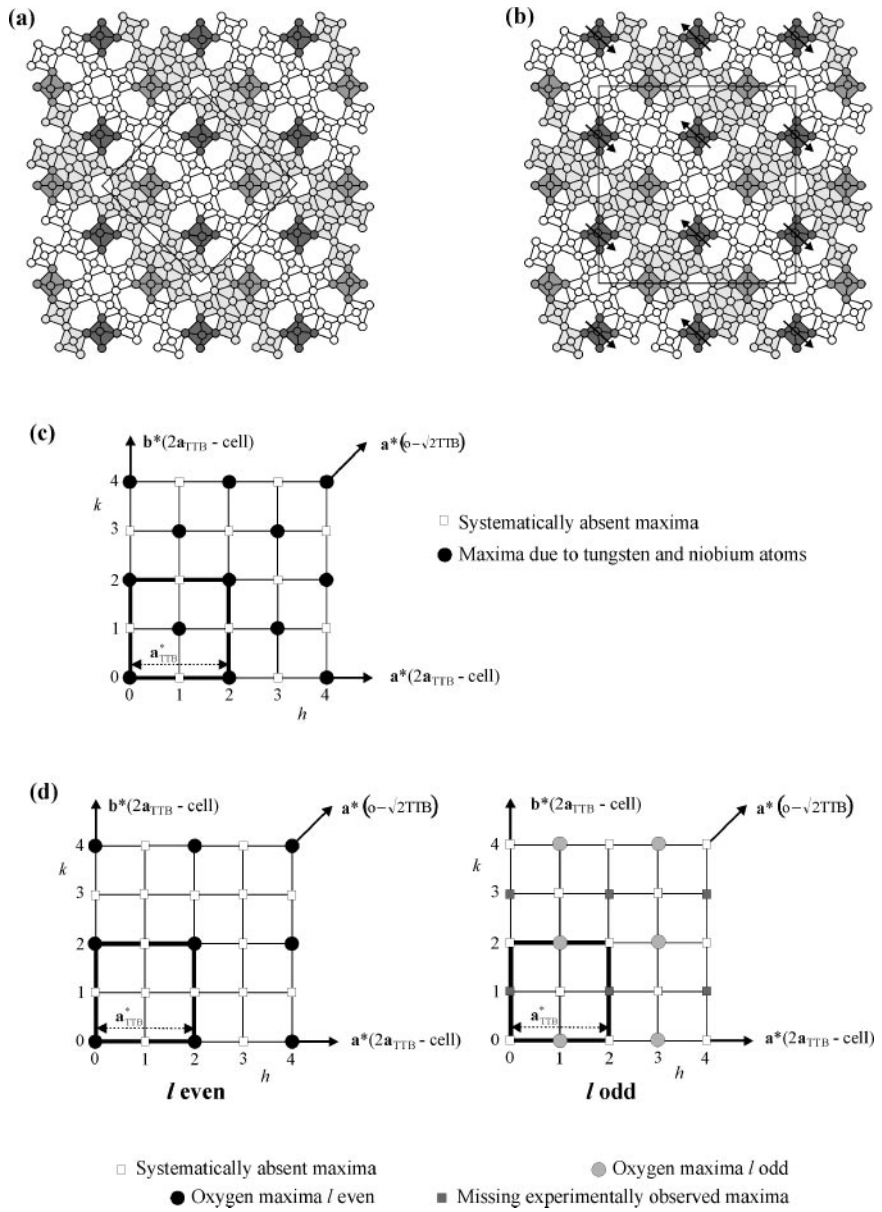

FIG. 9. (a) Framework structure of o-$\sqrt{}$2TTB. Light gray = PCs, medium gray = $M(2)O_6$ between a PC and PT, dark gray = $M(2)O_6$ between two PTs. (b) Model of one layer of the $2 \times 2 \times 2$ cell. In the second layer tilt directions are reversed. (c) Tungsten and niobium atom reciprocal space periodicity for even-order Laue levels. (d) Oxygen atom reciprocal space periodicity for even- and odd-order Laue levels. The heavy black line indicates the basic TTB repeat.

Thus for even-order layers, predicted maxima are identical to the first model, but for odd-order layers k must be odd and h even, thus generating the required missing reflections (Fig. 9d).

It is tempting to assume that reflections corresponding to the original o-$\sqrt{}$2TTB cell can be generated by multiple scattering, since some patterns did not possess these reflections and displayed only those corresponding to the supercell. However, if the addition rule for multiple scattering, $(h, k, l) = (h_1 + h_2, k_1 + k_2, l_1 + l_2)$, is to hold then there are no suitable reciprocal lattice vectors to generate these reflections. Nevertheless, there is another possible structure for the $2 \times 2 \times 2$ cell, shown in Fig. 10b, where the octahedral tilts are arranged such that an octahedron tilted in one direction is surrounded by octahedra tilted in the opposite sense. Considering this in terms of the $2 \times 2 \times 2$ cell, the cation framework is the same as for the other two models, but equivalent units in the anion framework are arranged at $(0, 0, 0)$, $(0, \frac{1}{2}, \frac{1}{2})$, $(\frac{1}{2}, 0, \frac{1}{2})$, and $(\frac{1}{2}, \frac{1}{2}, 0)$, so the anion framework is face-centered. Thus, for even-order layers the anions

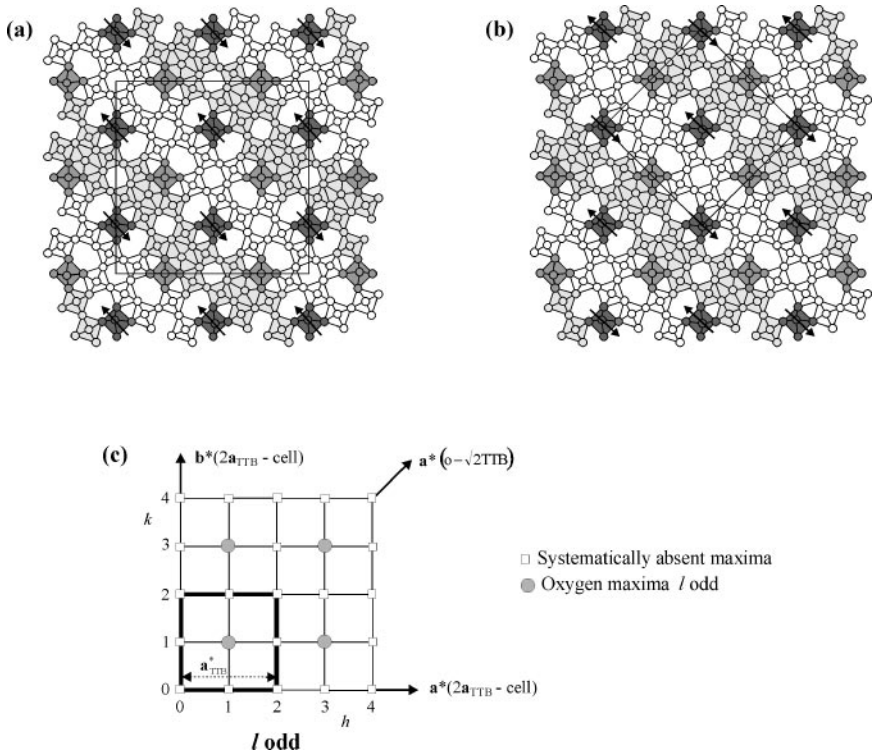

FIG. 10. (a) Model of one layer of a second $2 \times 2 \times 2$ supercell, with oxygen equivalent positions at (0, 0, 0), ($\frac{1}{2}$, 0, 0), (0, $\frac{1}{2}$, $\frac{1}{2}$), ($\frac{1}{2}$, $\frac{1}{2}$, $\frac{1}{2}$). In the second layer tilt directions are reversed. (b) Model for one layer of an anion lattice with a $\sqrt{2} \times \sqrt{2} \times 2$ supercell. (c) Oxygen atom reciprocal space periodicity for odd-order Laue levels of the $\sqrt{2} \times \sqrt{2} \times 2$ supercell. The heavy black line indicates the basic TTB repeat.

contribute only to the maxima of the basic TTB square (as in Fig. 9d), whereas on the odd-order layers they will generate reflections only in the middle of this square, as shown in Fig. 10c. This by itself will not generate all the possible maxima observed, but if multiple scattering occurs the vector in the even-order layers between reflections at the corners and the middle of the TTB square may then be used to generate spots at the corners of the TTB square in the layers with l odd.

It seems probable, therefore, that the true structure of o-$\sqrt{2}$TTB must consist of microdomains of all three arrangements of octahedral tilt. Evidence for twinning of the cation framework is directly observed in Fig. 4a, so it is reasonable that the anion framework would behave similarly, giving rise to the first two models, and the third case, which, judging from the relative intensities of the maxima observed on the odd-order layers, is much less common, will arise automatically where domains of the first two structures meet.

3.2. *Reduced Phases—Precursor Preparations*

Images and diffraction patterns recorded from the precursor compound confirmed the formation of the 3-TTB phase. Quantitative EDS measurements gave an average Nb:W ratio of 0.87 ± 0.05 (Table 3), which agrees well with the ideal value for $Nb_8W_9O_{47}$ of Nb:W = 0.89.

PXRD results from all precursor preparations were compared. In preparations carried out at 750°C, the pattern for the Pb = 0.03 sample was identical to that recorded from the precursor. For samples Pb = 0.34 to 1.35, however, the patterns were similar to each other but noticeably different from that of the precursor. In particular, peaks became

TABLE 3
EDS Results for Precursor Preparations

	Normalized average experimental compositions	
Reaction	Lead	Niobium
Precursor	—	Nb = 0.87 ± 0.05
Pb = 0.03/750°C	Pb = 0.03 ± 0.01	Nb = 0.90 ± 0.06[a]
Pb = 0.34/750°C	Pb = 0.29 ± 0.04	Nb = 0.90 ± 0.07[a]
Pb = 0.68/750°C	Pb = 0.34 ± 0.04	Nb = 0.88 ± 0.09
Pb = 1.35/750°C	Pb = 0.39 ± 0.07	Nb = 0.92 ± 0.10
Pb = 0.34/1000°C	Pb = 0.38 ± 0.03	Nb = 0.97 ± 0.05
Pb = 0.68/1000°C	Pb = 0.39 ± 0.03	Nb = 0.97 ± 0.07

[a] Small amounts of $Nb_8W_9O_{47}$ and WO_3 were also detected in these samples.

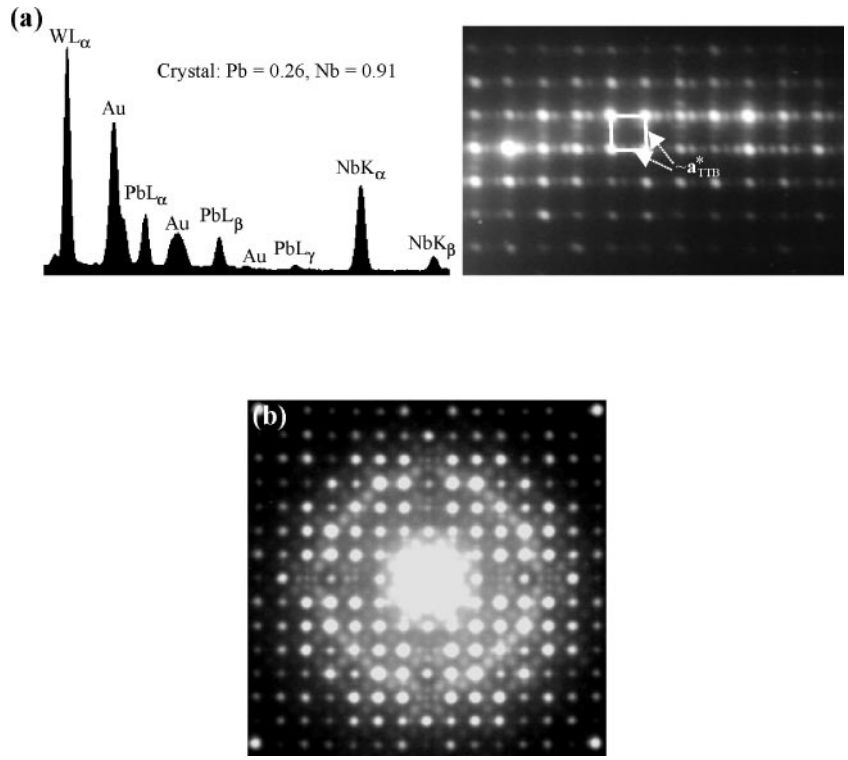

FIG. 11. (a) EDS spectrum and off-tilt diffraction pattern from sample Pb = 0.34/750°C, with a true bulk sample composition of Pb = 0.29 ± 0.04 and Nb = 0.90 ± 0.07 (gold specimen grid). (b) SAED pattern from a crystal of sample Pb = 0.34/750°C.

broader and more diffuse as the lead content increased, suggesting that the precursor structure was maintained for Pb = 0.03, but increasing lead content caused some structural modification. PXRD from samples Pb = 0.34 and 0.68 prepared at 1000°C appear identical to those recorded for Pb = 0.34 to 1.35 prepared at 750°C.

Quantitative EDS confirmed the formation of a quaternary Pb–Nb–W–O phase in all specimens, as shown in Table 3. The overall composition of the framework, as expressed by the Nb:W ratio, remains approximately constant throughout the series at approximately the value expected from the precursor composition. However, the quantity of lead detected increases with increasing nominal lead concentration. These observations support a "bronze-like" reduction of the precursor.

For preparations made at 750°C, the increase in nominal lead concentrations is not reflected in the relative compositional results, but instead the lead incorporation levels off and is a maximum for the nominally Pb = 1.35 specimen with an actual experimental value of Pb = 0.39 ± 0.07. This therefore represents the lead saturation composition, which is supported by the observation of excess unreacted lead in the samples with Pb = 0.68 and Pb = 1.35. Reaction at 1000°C achieves an identical value of the lead saturation, but this can be achieved without having to resort to such high nominal composition values. Residual lead was also detected in the Pb = 0.68 sample heated at this temperature.

Asymmetric SAED patterns recorded simultaneously with EDS analysis confirmed the presence of TTB-based quaternary phases for the whole compositional range. One such example is shown in Fig. 11a. Completely oriented

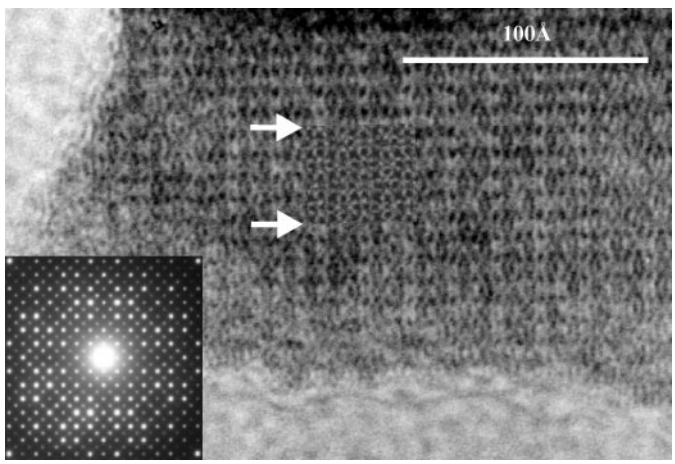

FIG. 12. Image and SAED pattern from sample Pb = 0.34/1000°C, displaying an ordered $\sqrt{2}$-TTB structure. Image simulation of o-$\sqrt{2}$TTB inset: 30 Å, $\Delta f = -300$ Å.

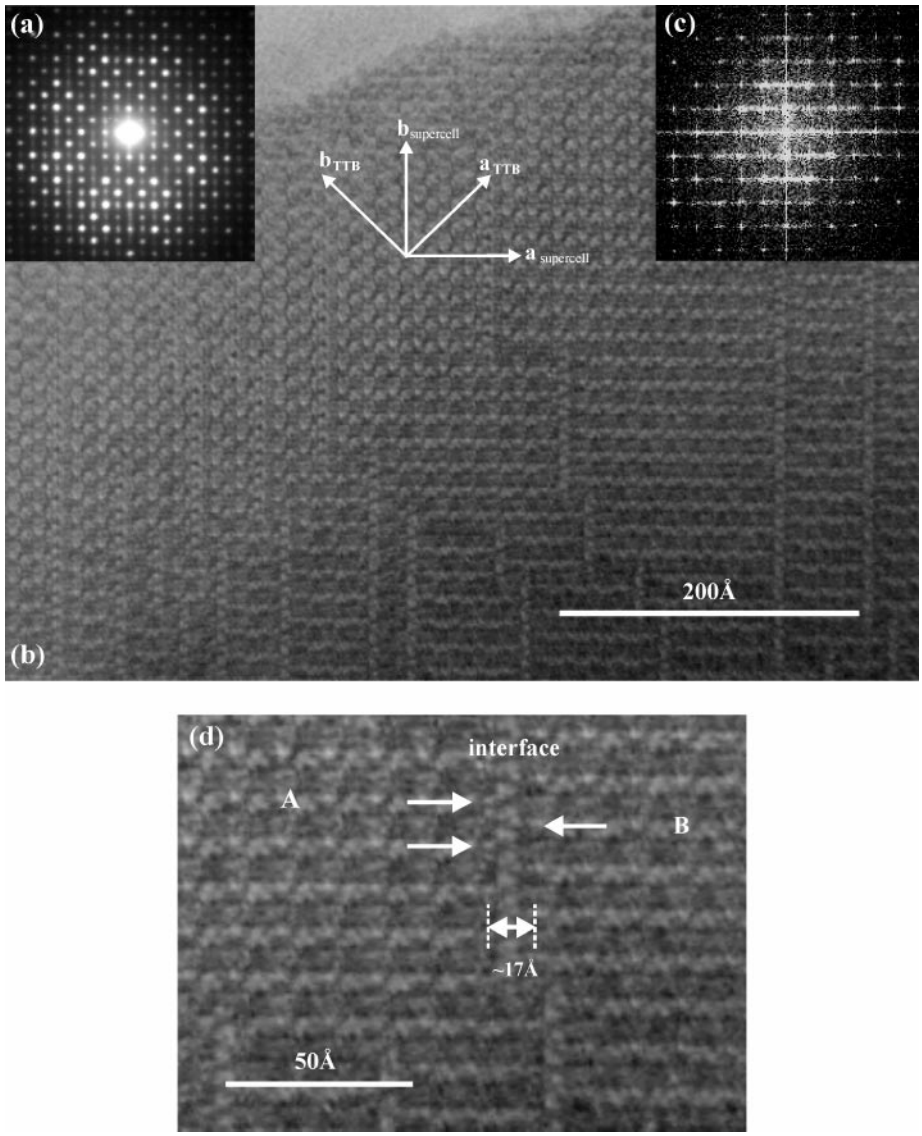

FIG. 13. (a) SAED pattern, (b) image, and (c) power spectrum of a crystal from sample Pb = 0.68/1000°C, showing a twinned and disordered $\sqrt{2}$-TTB structure. (d) Enlargement of (b) showing the interface between two domains (A and B) of o-$\sqrt{2}$TTB.

patterns from the Pb = 0.03 specimen heated at 750°C confirmed the formation of the quaternary 3-TTB phase. In a manner similar to patterns from the precursor sample, superstructure spots in the 3-TTB patterns were often found to be slightly diffuse. 3-TTB-type SAED patterns were also recorded from the Pb = 0.34 sample after heating at 750°C, but in addition, however, some patterns were recorded where the 3-TTB superlattice maxima had been replaced by diffuse patches of intensity at the $\sqrt{2}a^*$ position of each TTB subcell square, while the reflections due to the TTB subcell remained unchanged, as shown in Fig. 11b. SAED patterns similar to the latter were recorded from Pb = 0.68 and 1.35 phases where the heating temperature was 750°C.

Electron diffraction from the preparations made at 1000°C exhibited no 3-TTB periodicities but instead showed sharp reflections at the center of each square of the TTB subcell, indicating the formation of a $\sqrt{2}$-TTB-type superstructure. This is indicated in Fig. 12. Some patterns also displayed a streaking of the $\sqrt{2}$-TTB superstructure reflections along the [110] direction of the original TTB reciprocal lattice (Fig. 13a). The implied disorder in the structure is reflected in the corresponding image, as shown in Fig. 13b. Crystals of this $\sqrt{2}$-TTB phase also exhibited the $2a_{\mathrm{TTB}} \times 2b_{\mathrm{TTB}} \times 2c_{\mathrm{TTB}}$ superstructure which was observable only on odd-order Laue layers, in a manner identical to that found with the fully oxidized compounds.

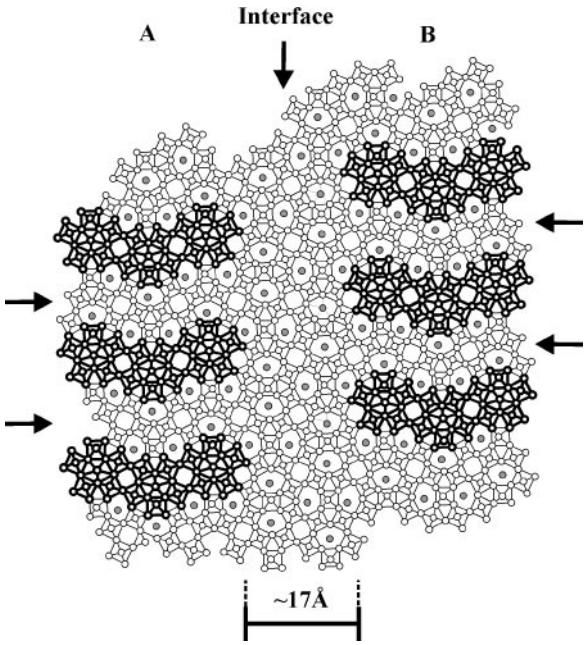

FIG. 14. Model of the interface between domains A and B. Heavy lines = PCs, gray circles = filled PTs. Arrows indicate the chains of unoccupied square tunnels between the double PT slabs, responsible for strong white contrast in image simulations of o-$\sqrt{2}$TTB at and around the Gaussian focus.

Discussion. [001] projection diffraction patterns recorded from the high-T $\sqrt{2}$-TTB phase strongly resembled those recorded from the fully oxidized o-$\sqrt{2}$TTB phase, and in addition the same complex supercell periodicity was observed. Image simulations (shown in Fig. 12) confirmed the high-T reduced phase as possessing the o-$\sqrt{2}$TTB structure. o-$\sqrt{2}$TTB formation is logical since this structure is able to accommodate more lead than the 3-TTB structure.

Structure factor calculations for the $2 \times 2 \times 2$ supercell of o-$\sqrt{2}$TTB determined that only $(MO)_n^{PC}$ and M framework atoms contribute to the $\sqrt{2}a^*_{TTB}$ superstructure reflection in the zero-order Laue layer, implying that the observed streaking of $\sqrt{2}a^*_{TTB}$ along $[110]_{TTB}$ (Fig. 13a) results from a disorder among the distribution of PCs within the crystal. The image from this crystal (Fig. 13b) indicates that streaking is caused by the formation of small domains of the o-$\sqrt{2}$TTB structure separated by fault planes.

The contrast of an enlargement of this image (Fig. 13d) is similar to that found in images recorded from crystals of the fully oxidized o-$\sqrt{2}$TTB structure (Figs. 3 and 4a), although the latter are generally from much thinner crystals. In the image simulation of o-$\sqrt{2}$TTB in Fig. 6 the defocus position is such that dark contrast corresponds to filled PT and PC sites. Furthermore, comparison of the simulation with the structure model also reveals that the strongest white contrast corresponds to the chains of unoccupied square tunnels situated between the double slabs of lead-filled PTs. It may therefore be deduced that the strong white lines in Fig. 13d highlight the position of the PTs. The width of the interface observed is around one o-$\sqrt{2}$TTB unit cell, which corresponds to a gap in the PC distribution and a slab of doubled PTs running perpendicular to domains A and B (Fig. 14). The observed offset of the domains across the interface is approximately one-half of the vertical cell repeat, which agrees with the proposed model.

The formation of such an interface results in a local increase in the total number of PTs, implying that the o-$\sqrt{2}$TTB structure reconstructs to form these boundaries in order to increase its incorporation of lead. This is supported by the observation of deposits of residual lead in both high-T preparations after heating. The presence of excess lead during synthesis could have encouraged such local structural modifications to develop.

Low-temperature preparations. It appears that small amounts of lead are initially incorporated into the 3-TTB structure at lower temperatures without any significant structural consequences. However, the progressive loss of the 3-TTB periodicity with increasing lead incorporation observed for experiments at these temperatures suggests that partial recrystallization of the precursor occurs during synthesis. It is unlikely that the TTB framework would break up completely at 750°C, given the high temperatures required for the formation of 3-TTB itself (7, 8), and the fact that TTB reflections are constant features of all the diffraction patterns. However, 750°C appears sufficient to cause disorder among the M atoms forming PCs. Upon heating, the 3-TTB PC distribution randomizes as the framework is reduced and incorporates lead, and the emerging $\sqrt{2}$-TTB periodicity seen in some diffraction patterns is almost certainly caused by an embryonic semiordered o-$\sqrt{2}$TTB phase. The duration of synthesis employed in these experiments was not sufficient to enable a full conversion of the products to o-$\sqrt{2}$TTB but it is possible that more extended annealing of these preparations would ultimately produce an ordered o-$\sqrt{2}$TTB phase.

3.3. Reduced Phases—Component Preparations

PXRD patterns for the component preparations appeared identical to that for the 3-TTB precursor. Quantitative EDS (Table 4) indicated experimental Nb and W compositions which were in good agreement with their nominal values. No residual lead was observed in the samples after heating, indicating that this metal was completely accommodated in all reactions. The Pb = 0.03 preparation was found to be biphasic, displaying both $Nb_8W_9O_{47}$ and a quaternary lead-containing phase, but other preparations showed only a quaternary phase. Off-tilt diffraction patterns recorded during EDS experiments indicated that the

TABLE 4
EDS Results for Component Preparations

Reaction	Normalized average experimental compositions	
	Lead	Niobium
Pb = 0.03/2 days	Pb = 0.05 ± 0.03	Nb = 0.88 ± 0.08
	Pb = 0.00 ± 0.01	Nb = 0.85 ± 0.10
Pb = 0.09/2 days	Pb = 0.09 ± 0.03	Nb = 0.86 ± 0.08
Pb = 0.09/7 days	Pb = 0.09 ± 0.02	Nb = 0.90 ± 0.10

Note. Results normalized to a tungsten composition of 1 mole.

quaternary phase had a 3-TTB structure in all three preparations (Fig. 15a).

HREM examination confirmed the formation of a 3-TTB quaternary phase in all samples. After 2 days of heating, crystals were invariably partially disordered and the 3-TTB superstructure reflections in SAED patterns were slightly diffuse (Fig. 15b). Images recorded from the sample with Pb = 0.09 and heated for 7 days indicated a more ordered 3-TTB superstructure, typified by sharp superstructure reflections and an absence of any twinning. No doubled-*c* periodicity was observed for either ternary 3-TTB or its related quaternary phases.

4. CONCLUSIONS

For the fully oxidized phases, where both niobium and lead contents were gradually increased, the structural progression in the product was very clear. Initially, the 3-TTB superstructure was formed, but as the lead and niobium content increased the structure type changed to o-$\sqrt{2}$TTB, which has potentially more PTs available to accommodate the Pb^{2+} ions. Ultimately, however, even this number of PTs proved insufficient, and PCs were then converted into PTs, resulting in a structure which more closely resembled the simple TTB phase. Compositional analysis indicated that the maximum number of Pb^{2+} ions situated in each PT was approximately 0.5, and the unit cell of the o-$\sqrt{2}$TTB phase was found to be doubled in the *c* direction.

The behavior of the reduced phases was remarkably similar, although the extent of the lead substitution was not taken as far. For those produced from the 3-TTB precursor ($Nb_8W_9O_{47}$) the 3-TTB structure was initially maintained in the quaternary phase, but soon converted at high temperature to the o-$\sqrt{2}$TTB phase in an exactly analogous manner as for the fully oxidized phases. Preparations made at lower temperatures indicated the same basic features, although the rate of reaction was much slower and the equilibrium assemblage was not reached in the heating times employed. Reduced phases prepared by the component route demonstrated that it is possible to form non-stoichiometric reduced PT/PC phases that retain the framework of the oxidized parent structure. The substitution of lead was not taken far enough to determine the maximum lead incorporation tolerated before framework restructuring occurs. The results from precursor preparations

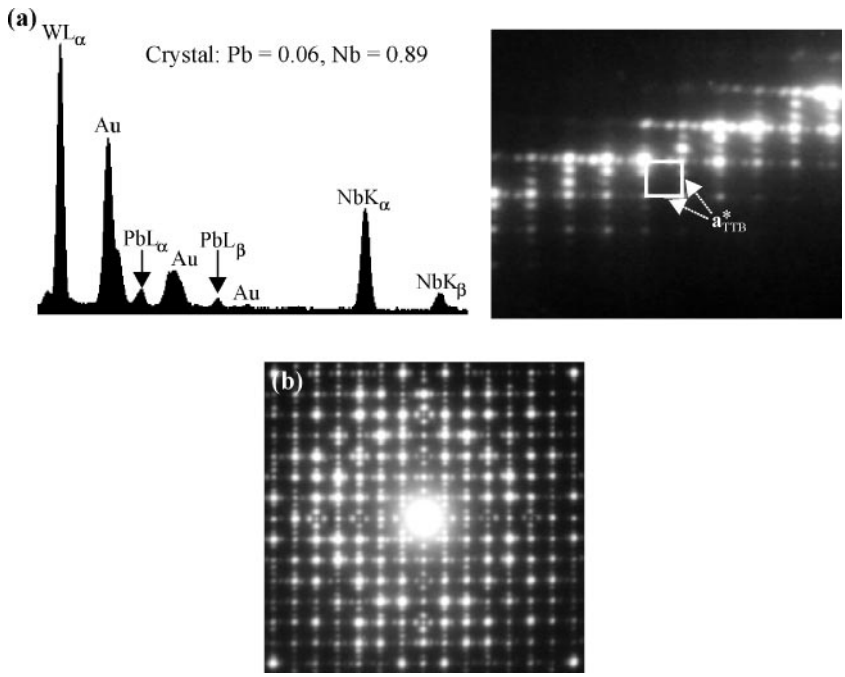

FIG. 15. (a) Example SAED pattern and EDS spectrum from sample Pb 0.09/2 days with true average composition Pb = 0.09 ± 0.03 and Nb = 0.86 ± 0.08 (gold specimen grid). (b) Example SAED pattern, sample Pb = 0.03/2 days.

suggest that the o-$\sqrt{}$2TTB structure may form at higher compositions.

The similarity in behavior shown by fully oxidized and reduced phases is initially quite surprising, and indicates that the main structure-determining factor is the size of the species to be accommodated, rather than its oxidation state. This also implies that, whatever the initial oxidation state, lead is invariably incorporated into the structure as Pb^{2+} ions, and any excess electrons resulting in the reduced phases go into the unoccupied bands of the tungsten and niobium atoms. It therefore appears that the pentagonal columns displayed by all these structures are just as capable of accommodating metal–oxygen chains, with the metal atom at the same level as those in the surrounding octahedra, and Pb^{2+} ions at an intermediate level, where the maximum oxygen coordination number can be as high as 10. The only significant difference seems to be that, whereas framework metal ions can be inserted into each plane of octahedra, electrostatic repulsion considerations necessitate the incorporation of Pb^{2+} at alternate layers. There is no evidence from these studies that some tunnels may be occupied partly by metal–oxygen chains, and partly by Pb^{2+}, but this must remain a possibility, and any technique which determines the structure in projection only, as is the case with electron diffraction and HREM, cannot resolve this question.

Electron diffraction studies indicated that the doubling of the *c* repeat in the o-$\sqrt{}$2TTB structure did not appear to depend on the extent of lead substitution, so it must be concluded that this doubling is due to octahedral tilting rather than ordering of the Pb^{2+} ions. This is in accordance with findings in the basic TTB phases, although the arrangement of octahedral tilts is different, but the scheme described above can explain the pattern of superlattice maxima appearing on the odd-order levels in reciprocal space. Given the varying degree of lead substitution, this therefore suggests that the octahedral framework of these structures is sufficiently rigid to impose such tilting schemes no matter what the composition of the structure is in terms of filled PTs. At first sight it is then surprising that $Nb_8W_9O_{47}$ converts so readily to the o-$\sqrt{}$2TTB phase when incorporating lead, indicating that, in terms of PCs and PTs, structural rearrangement is relatively facile, but these structures, and the basic TTB phase, contain an identical arrangement of tunnels, so conversion of a PC to a PT is largely a matter of diffusion of metal and oxygen via the octahedron separating adjacent tunnels. Indeed, the framework of octahedra can be thought of as continuous throughout all the structures, and where domains exist of one phase within another, such as the coexistence of 3-TTB and o-$\sqrt{}$2TTB, the only modification present is the octahedral tilting which occurs in the latter, but which is apparently prevented from occurring by the more evenly distributed arrangement of PCs in the former.

ACKNOWLEDGMENTS

The authors express thanks to the E.P.S.R.C., for providing microscope facilities, and to the Isaac Newton Trust and JEOL (UK) for financial support to S.K.H.

REFERENCES

1. L. Bartha, A. B. Kiss, and T. Szalay, *Int. J. Refractory Metals Hard Mater.* **13,** 77–91 (1995).
2. R. D. J. Tilley, *Int. J. Refractory Metals Hard Mater* **13,** 93–109 (1995).
3. G. Hägg, *Nature* **135,** 847 (1935); *Z. Phys. Chem. B* **29,** 192 (1935).
4. A. Magnéli, *Ark. Kemi* **1,** 213 (1949).
5. A. Magnéli, *Acta Chem. Scand.* **7,** 315–324 (1953).
6. A. Hussain and L. Kihlborg, *Acta Crystallogr. A* **32,** 551 (1976).
7. R. S. Roth and A. D. Wadsley, *Acta Crystllogr.* **19,** 26 (1965).
8. R. S. Roth and J. L. Waring, *J. Res. Natl. Bur. Stand.* **70A,** 281–303 (1966).
9. A. D. Wadsley, *in* "Non-Stoichoimetric Compounds" (L. Mandelcorn, Ed.), Academic Press, New York, 1964.
10. M. Lundberg, *Chem. Commun. Univ. Stockholm*, No. XII (1971).
11. M. Lundberg, M. Sundberg, and A. Magnéli, *J. Solid State Chem.* **44,** 32–40 (1982).
12. L. A. Bursill and B. G. Hyde, *Nature Phys. Sci.* **240,** 122 (1972).
13. B. G. Hyde and M. O'Keeffe, *Acta Crystallogr. A* **29,** 243 (1973).
14. H. Obayashi and J. S. Anderson, *J. Solid State Chem.* **17,** 79–89 (1976).
15. S. Horiuchi, K. Muramatsu, and Y. Matsui, *J. Appl. Crystallogr.* **13,** 141–147 (1980).
16. F. Krumeich, *Acta Crystallogr. B* **54,** 240–249 (1998).
17. A. W. Sleight, *Acta Chem. Scand.* **20,** 1102–1112 (1966).
18. S. Iijima and J. G. Allpress, *Acta Crystallogr. A* **30,** 22 (1974).
19. S. Iijima and J. G. Allpress, *Acta Crystallogr. A* **30,** 29 (1974).
20. M. Lundberg, *Acta Crystallogr.* **26,** 2932–2940 (1972).
21. M. Lundberg and M. Sundberg, *Ultramicroscopy* **52,** 429–435 (1993).
22. M. Sundberg and M. Lundberg, *Acta Crystallogr. B* **43,** 429 (1987).
23. M. Sundberg and M. Lundberg, *Chem. Scr.* **28,** 77–80 (1988).
24. T. Hörlin, B.-O. Marinder, and M. Nygren, *Rev. Chim. Miner.* **19,** 231 (1982).
25. M. Sundberg and B.-O. Marinder, *J. Solid State Chem.* **84,** 23–38 (1990).
26. B.-O. Marinder and M. Sundberg, *Acta Crystallogr. C* **40,** 1303–1306 (1984).
27. M. Lundberg and M. Sundberg, *Chem. Scr.* **28,** 81–87 (1988).
28. M. Lundberg and M. Sundberg, *J. Less Common Met.* **137,** 163–179 (1988).
29. M. J. Sayagués, J. L. Hutchinson, and F. Krumeich, *J. Solid State Chem.* **143,** 33–40 (1999).
30. M. Lundberg and M. Sundberg, *J. Solid State Chem.* **63,** 216 (1986).
31. S. M. Montemayor, A. A. Mendez, A. Martínez-de la Cruz, A. F. Fuentes, and L. M. Torres-Martínez, *J. Mater. Chem.* **8,** 2777–2781 (1998).
32. R. A. Bernoff and L. E. Conroy, *J. Am. Chem. Soc.* **82,** 6261 (1960).
33. T. Ekström and R. D. J. Tilley, *J. Solid State Chem.* **24,** 209–218 (1978).
34. S. T. Triantafyllou, P. C. Christidis, and Ch. B. Lioutas, *J. Solid State Chem.* **130,** 176–183 (1997).
35. M. H. Francombe and B. Lewis, *Acta Crystallogr.* **11,** 696 (1958).
36. Ph. Labbé, M. Frey, and G. Allais, *Acta Crystallogr. B* **29,** 2204–2210 (1973).
37. Ph. Labbé, M. Frey, B. Raveau, and J. C. Monier, *Acta Crystallogr. B* **33,** 2201–2212 (1977).
38. D. A. Jefferson, J. M. Thomas, G. R. Millward, K. Tsuno, A. Harriman, and R. D. Brydson, *Nature* **323,** 428–431 (1986).

39. P. J. Hewitt, D. A. Jefferson, G. R. Millward, and K. Tsuno, *JEOL News* **27,** 2–9 (1989).
40. D. A. Jefferson, G. R. Millward, and J. M. Thomas, *Acta Crystallogr. A* **32,** 823 (1976).
41. S. K. Haydon, Ph.D. Thesis, University of Cambridge, 2000.
42. R. D. Shannon and C. T. Prewit, *Acta Crystallogr. B* **25,** 925–946 (1969).
43. F. Takusagawa and R. A. Jacobson, *J. Solid State Chem.* **18,** 163–174 (1976).
44. R. Steadman, *Mater. Res. Bull.* **7,** 1143–1150 (1972).
45. M. Goreaud, Ph. Labbé, Y. Monfort, and B. Raveau, *Rev. Chim. Miner.* **17,** 79 (1980).
46. P.-J. Lin and L. A. Bursil, *Acta Crystallogr. B* **43,** 504–512 (1987).
47. H.-Y. Lee and R. Freer, *J. Appl. Crystallogr.* **31,** 683–691 (1988).